

An integrated Sachs-Wolfe effect vs redshift test for the cosmological parameters

R. Kantowski,^{1,*} B. Chen,^{2,†} and X. Dai^{1,‡}

¹*Homer L. Dodge Department of Physics and Astronomy,
University of Oklahoma, 440 West Brooks, Norman, OK 73019, USA*

²*Research Computing Center, Department of Scientific Computing,
Florida State University, Tallahassee, FL 32306, USA*

(Dated: March 17, 2015)

Abstract

We describe a method using the integrated Sachs-Wolfe (ISW) effect caused by individual inhomogeneities to determine the cosmological parameters, H_0 , Ω_m , and Ω_Λ , etc. This ISW-redshift test requires detailed knowledge of the internal kinematics of a set of individual density perturbations, e.g., galaxy clusters and/or cosmic voids, in particular their density and velocity profiles, and their mass accretion rates. It assumes the density perturbations are isolated and imbedded (equivalently compensated) and makes use of the newly found relation between the ISW temperature perturbation of the CMB and the Fermat potential of the lens. Given measurements of the amplitudes of the temperature variations in the CMB caused by such clusters or voids at various redshifts and estimates of their angular sizes or masses, one can constrain the cosmological parameters. More realistically, the converse is more likely, i.e., if the background cosmology is sufficiently constrained, measurement of ISW profiles of clusters and voids (e.g., hot and cold spots and rings) can constrain dynamical properties of the dark matter, including accretion, associated with such lenses and thus constrain the evolution of these objects with redshift.

PACS numbers: 98.62.Sb, 98.65.Dx, 98.80.-k

Keywords: General Relativity; Cosmology; Gravitational Lensing;

I. INTRODUCTION

The late time integrated Sachs-Wolfe (ISW) effect [1], also called the Rees-Sciama (RS) effect [2], has recently been suggested (as well and disputed) as the source of observed hot and cold spots in the CMB temperature around some known large scale structures—galaxy clusters and cosmic voids [3–5]. By modeling cluster and void density profiles, and by adjusting cluster masses and void depths, observed temperature excesses/deficits can be matched by ISW predictions [6–11]. Several proposals also exist to use lensing of the CMB to determine properties of these clusters and voids as well as the cosmological parameters [12–15]. What we present in this paper is not unrelated to these proposals but offers an easier and more direct method for relating the ISW temperature shifts to the cluster/void

* kantowski@ou.edu

† bchen3@fsu.edu

‡ xdai@ou.edu

structure and the background cosmology. The conventional approach to determine the ISW effect is to first construct the “lensing potential” of a cluster or void from a model of its density profile and then compute the potential’s effect on the observed CMB’s temperature. Our approach uses another lensing quantity, the “Fermat potential” or equivalently the potential part of the time delay, to relate the lens and cosmology to the ISW temperature fluctuations. Our method of evaluating the ISW effect is directly related to the lens’ mass profile and is more transparent than the conventional approach. It is simpler to use and requires the construction of only one single function, the potential part of the time delay [16]. It is also flexible to use, i.e., the lens structure and/or its evolution can easily be varied and the effects of either are separately discerned.

We have recently developed the embedded lens theory [17–23] which could be called the Swiss cheese lens theory, or at lowest order, the compensated lens theory. The theory originated from the Swiss cheese models of general relativity (GR) [24–26], therefore one can be confident of its gravitational predictions, if GR is indeed the correct theory. An embedded lens at redshift z_d is constructed by first removing a comoving sphere of radius χ_b from a homogeneous Friedman-Lemaître-Robertson-Walker (FLRW) cosmology producing a Swiss cheese void, see Fig. 1. The void has a physical radius $r_d = \chi_b R(t_d)$ at cosmic time t_d that expands with the radius of the background cosmology $R(t)$ but has a constant angular radius θ_M as seen by an observer, as the observer ages. In the lowest order lensing theory [19] these radii are related (by embedding) to the Schwarzschild radius r_s of the removed mass M_d by

$$\theta_M = \frac{r_d}{D_d} = \frac{1}{1+z_d} \frac{1}{D_d} \left(\frac{r_s}{\Omega_m} \frac{c^2}{H_0^2} \right)^{1/3}, \quad (1)$$

where D_d is the angular diameter distance of the void’s center in the background cosmology (e.g., a standard FLRW cosmology), H_0 the Hubble constant, and Ω_m the matter density parameter. The total mass removed M_d is next replaced with any appropriate spherical density while keeping Einstein’s equations satisfied throughout the Swiss cheese void and on its time-evolving boundary. The logic for embedding is simple, by computing the mean density inside larger and larger spheres centered on a density perturbation, a radius will be reached beyond which the mean density coincides with the FLRW background. The minimum radius at which this takes place can be chosen as r_d . The simplest such exact Swiss cheese models are constructed by filling the void with one of the Lemaître-Tolman-

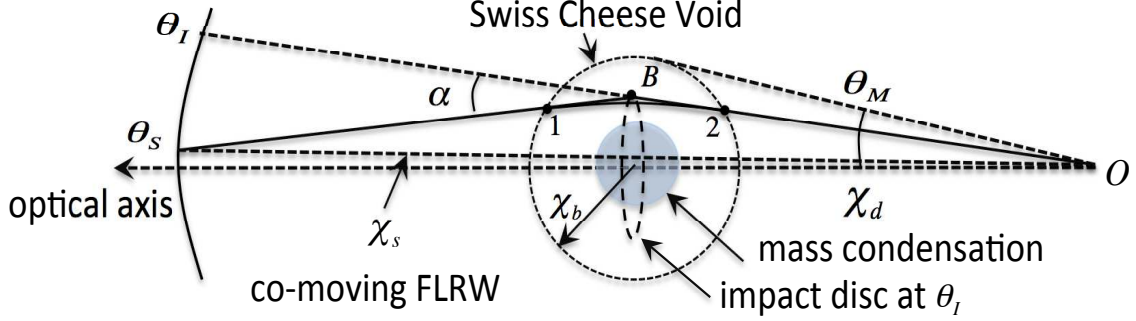


FIG. 1. The comoving geometry of an embedded lens at redshift $1 + z_d = R_0/R(t_d)$. Angles θ_s and θ_I respectively, are source and image angles; χ_d and χ_s are the comoving angular distances of the lens and the source. The (constant) angular size of the void, in lowest order lensing theory, is $\theta_M \equiv \chi_b/\chi_d$ where χ_b is the comoving radius of the Swiss cheese void. The physical radius of the deflecting lens depends on the cosmic time t_d , i.e., $r_d = R(t_d)\chi_b$. The shadowed area represents an embedded cluster. The dashed circle shows the impact disc of angular radius θ_I , used to compute the included projected mass fraction $f(x)$ of the lens, see Eq. (2). The equivalent figure for a void lens has a mass condensation surrounding a low density central region and a repulsive instead of attractive deflection angle α .

Bondi (LTB) models [27–29]. Since we are only interested in the lowest order lensing theory, any non-relativistic fluid whose net mass is the same as the removed Swiss cheese void’s mass M_d will suffice. Consequently, models of physical voids must be surrounded by higher density regions and cluster models surrounded by lower density regions. Such linearized gravitational models are often referred to as compensated [30–35].

For spherical density perturbations we have shown in [21, 22] that to lowest order an embedded lens can be completely described by its Fermat potential (equivalent to the sum of the geometrical and potential time delays, $cT = cT_g + T_p$)

$$cT(\theta_s, \theta_I) = (1 + z_d) \frac{D_d D_s}{D_{ds}} \left[\frac{(\theta_s - \theta_I)^2}{2} + \theta_E^2 \int_x^1 \frac{f(x', z_d) - f_{\text{RW}}(x')}{x'} dx' \right]. \quad (2)$$

Here $x \equiv \theta_I/\theta_M$ is the normalized image angle, $f(x) \equiv M_{\text{disc}}(\theta_I)/M_{\text{disc}}(\theta_M)$ is the fraction of the embedded lens’ mass projected within the impact disc of angular radius θ_I , and $f_{\text{RW}}(x) = 1 - (1 - x^2)^{3/2}$ is the corresponding quantity for the removed co-moving FLRW dust sphere. At (and beyond) the boundary of the embedded lens, $f(x) = f_{\text{RW}}(x) = 1$. The angle $\theta_E = \sqrt{2r_s D_{ds}/D_d D_s}$ is the usual Einstein ring angle. Distances D_s and D_{ds}

are angular diameter distances to the source measured from the observer and the deflector, respectively. The geometrical part of the time delay T_g , i.e., the first term in Eq. (2), has a universal form whereas the potential part T_p depends on the individual lens structure. To construct the Fermat potential all that is needed is a mass density profile $\rho(r, z_d)$ for which

$$cT_p(\theta_I, z_d) = 2(1 + z_d)r_s \int_x^1 \frac{f(x', z_d) - f_{\text{RW}}(x')}{x'} dx', \quad (3)$$

can be integrated. All embedded lens properties can be constructed once the specific $T_p(\theta_I, z_d)$ is known. For example the specific lens equation is given by a θ_I -variation $\delta T(\theta_S, \theta_I)/\delta \theta_I = 0$. In [22] we have shown that the ISW effect [1, 2] is obtained by a z_d -derivative of T_p (or T since $\partial T_g/\partial z_d \equiv 0$)

$$\frac{\Delta \mathcal{T}(\theta_I, z_d)}{\mathcal{T}} = H_d \frac{\partial T_p(\theta_I, z_d)}{\partial z_d}. \quad (4)$$

In this expression $\Delta \mathcal{T}$ is the change in the CMB's temperature \mathcal{T} caused by CMB photons passing through an evolving gravitational lens at impact angle θ_I . The cosmic-time evolution of the lens is replaced by a dependence on the redshift z_d at which it is seen and the Hubble parameter at that redshift is denoted by $H_d = H(z_d)$. To compute the ISW effect caused by an embedded lens, we need not only the density profile as required by conventional lens theory [36] to compute image properties, but we also need the density profile's evolution rate to compute the z_d -derivative. Because Eq. (4) contains only a first derivative we do not need to know the lens' history (i.e., the dynamics of its motion), only its density profile and its velocity distribution at lensing time z_d .

A somewhat different connection between the ISW effect and lensing, other than the relation of Eq. (4) to Eq. (2), has been noted by prior analytic work. While investigating corrections to the linear ISW effect caused by keeping nonlinear terms in the dark matter momentum density, [37–39] found a term in the time derivative of the lensing potential (the integral of which is conventionally used to compute the ISW effect) that depends on the local deflection angle and the local transverse motion of the gravitational lens. This term is reminiscent of the transverse Doppler effect that produces a dipole signal in the CMB, i.e., the Birkinshaw-Gull effect [40, 41]. Even though Eqs. (2)–(4) are tailored for spherical lenses whose centers don't move transversely relative to the CMB, their evolving projected mass densities $(2\pi x)^{-1}df/dx$ are associated with radially directed divergent momentum densities. That motion would produce local effects on the transiting photons that could be similarly identified if analyzed conventionally using the lensing potential as done by [37–39].

II. THE PRINCIPLE BEHIND THE ISW-Z TEST

Equation (4) gives the fluctuation in the observed CMB temperature as a function of angular position across a given, possibly evolving, density perturbation (a lens) caused by the ISW effect. From Eq. (4) the ISW signal is seen to depend on the lens' redshift z_d , its mass r_s , its projected fractional density profile $f(x, z_d)$ (including its evolution, i.e., its first derivative with respect to redshift), as well as the background cosmology. We construct the new cosmology test using this simple relation. By splitting Eq. (4) into an amplitude term proportional to the product of the lens mass and the Hubble parameter, times a lens structure dependent term $\mathcal{S}(\theta_I, z_d)$ we have

$$\frac{\Delta\mathcal{T}(\theta_I, z_d)}{\mathcal{T}} = 2r_s \frac{H_d}{c} \times \mathcal{S}(\theta_I, z_d), \quad (5)$$

where the lens structure dependent term is defined by

$$\mathcal{S}(\theta_I, z_d) \equiv \frac{\partial}{\partial z_d} \left[(1 + z_d) \int_x^1 \frac{f(x', z_d) - f_{\text{RW}}(x')}{x'} dx' \right]. \quad (6)$$

If the lens mass and structure are known, the amplitude of $\Delta\mathcal{T}(\theta_I, z_d)/\mathcal{T}$ at the lens' center ($\theta_I = 0$) can in principle be used to determine the Hubble parameter $H(z_d)$. In practice, to apply Eq. (5) to a cold or hot spot associated with a single void or cluster lens it must be averaged over the aperture of the detector, i.e., $\Delta\mathcal{T}(\theta_I, z_d)$ and $\mathcal{S}(\theta_I, z_d)$ are replaced by their averaged values, $\Delta\mathcal{T}(z_d)$ and $\mathcal{S}(z_d)$. If a set of clusters and/or voids can be found whose redshifts, masses, and evolving structures can be determined, then $\mathcal{S}(\theta_I, z_d)$ and $\mathcal{S}(z_d)$ can be determined. Given the CMB temperature data at the positions of these clusters and/or voids, Eq. (5) will determine the Hubble parameter H_d as a function of z_d . The redshift dependent Hubble parameter can then be used to constrain all the cosmological parameters. In Sec. III we illustrate the procedure by applying it to simple top-hat cluster and void models.

The above form of the ISW-z test assumes the mass of the lensing cluster or void is known; however for cosmic voids, radii can be more easily determined than masses [42]. We now present a second form of the ISW-redshift test preferable for such voids. This second test requires knowledge of the energy content of the FLRW background before it can be applied. We construct this form of ISW-redshift test by looking at the central region of the void or cluster, eliminating r_s from Eq. (4) by using Eq. (1), and dividing by the cube of the

angular radius of the Swiss cheese void θ_M^3 to obtain the H_0 and r_s independent result

$$\frac{\Delta\mathcal{T}(z_d)/\mathcal{T}}{(\theta_M)^3} = \mathcal{C}(z_d) \times \mathcal{S}(z_d), \quad (7)$$

where the pure curvature dependent part $\mathcal{C}(z_d)$ is defined by

$$\mathcal{C}(z_d) \equiv 2\Omega_m \frac{H_d}{H_0} \left[(1+z_d) D_d \frac{H_0}{c} \right]^3, \quad (8)$$

and the lens structure dependent term $\mathcal{S}(z_d)$ is again defined by Eq. (6).

By replacing the Hubble parameter H_d and the angular diameter distance D_d by functions of the curvature and redshift, assuming for example a simple possibly evolving dark-energy Λ CDM like gravity source with $p_\Lambda/\rho_\Lambda c^2 = [w_0 + w_a z/(1+z)]$, we have

$$H_d/H_0 \equiv E(z_d) = \sqrt{\Omega_\Lambda (1+z_d)^{3(1+w_0+w_a)} e^{-3w_a z_d/(1+z_d)} + \Omega_m (1+z_d)^3 + (1-\Omega_m-\Omega_\Lambda)(1+z_d)^2}, \quad (9)$$

and

$$(1+z_d) D_d \frac{H_0}{c} = \frac{1}{\sqrt{|1-\Omega_m-\Omega_\Lambda|}} \text{Sinh} \left[\sqrt{|1-\Omega_m-\Omega_\Lambda|} \int_0^{z_d} \frac{dz}{E(z)} \right], \quad (10)$$

where $\text{Sinh}(x) = \sin(x)$, x , and $\sinh(x)$ for a closed, flat, or open universe, respectively. The conventional Λ CDM cosmology is recovered when $w_0 = -1$ and $w_a = 0$. The curvature part of Eq. (7) becomes

$$\mathcal{C}(z_d) \equiv 2\Omega_m E(z_d) \left\{ \frac{1}{\sqrt{|1-\Omega_m-\Omega_\Lambda|}} \text{Sinh} \left[\sqrt{|1-\Omega_m-\Omega_\Lambda|} \int_0^{z_d} \frac{dz}{E(z)} \right] \right\}^3. \quad (11)$$

The sensitivity of $\mathcal{C}(z_d)$ to the cosmological parameters can be seen by its series expansion for $z_d \ll 1$

$$\begin{aligned} \mathcal{C}(z_d) \approx 2\Omega_m z_d^3 & \left[1 - \frac{1}{2} \left(1 + \frac{1}{2}\Omega_m + \frac{1}{2}\Omega_\Lambda [1+3w_0] \right) z_d \right. \\ & \left. + \frac{1}{4} \left(3 - \Omega_m - [1-3w_0]\Omega_\Lambda + \frac{1}{4} (\Omega_m + \Omega_\Lambda [1+3w_0])^2 \right) z_d^2 + \mathcal{O}[z_d^3] \right]. \end{aligned} \quad (12)$$

It is obviously most sensitive to Ω_m and doesn't even depend on w_a to this order.

We plot the curvature part, Eq. (11), in the left panel of Fig. 2 for four familiar cosmologies as solid curves: the Einstein de Sitter (EdS) universe, $(\Omega_m, \Omega_\Lambda) = (1, 0)$; a dark matter only universe, $(\Omega_m, \Omega_\Lambda) = (0.3, 0)$; a Λ CDM universe, $(\Omega_m, \Omega_\Lambda) = (0.3, 0.7)$; and a baryonic matter only universe, $(\Omega_m, \Omega_\Lambda) = (0.05, 0)$. We also indicate the range of variation in

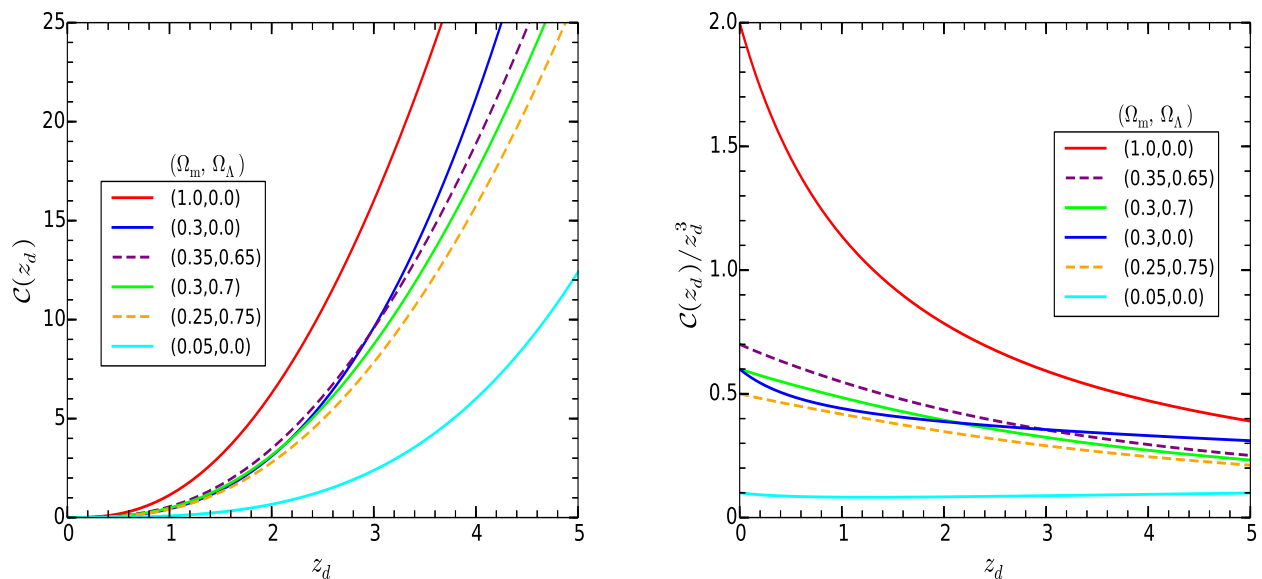


FIG. 2. Plots of the curvature term $\mathcal{C}(z_d)$ from Eq. (11) for four background cosmologies (the solid curves from top to bottom): the Einstein de Sitter universe, $(\Omega_m, \Omega_\Lambda) = (1, 0)$, red; a dark matter only universe, $(\Omega_m, \Omega_\Lambda) = (0.3, 0)$, blue; a Λ CDM universe, $(\Omega_m, \Omega_\Lambda) = (0.3, 0.7)$, green; and a baryonic matter only universe, $(\Omega_m, \Omega_\Lambda) = (0.05, 0)$, cyan. The two dashed curves show the extent to which $\mathcal{C}(z_d)$ varies for small changes about $(\Omega_m, \Omega_\Lambda) = (0.3, 0.7)$. In the right panel the small z_d dependence is factored out.

$\mathcal{C}(z_d)$ for flat Λ CDM models by plotting, as dashed curves, the $(\Omega_m, \Omega_\Lambda) = (0.35, 0.65)$ and $(0.25, 0.75)$ cases. In the right panel of Fig. 2 we plot these same curves but with the common factor z_d^3 divided out, i.e., $\mathcal{C}(z_d)/z_d^3$. A significant dependence on Ω_m is easily seen.

In Fig. 3 we show the accuracy of the series approximation for $\mathcal{C}(z_d)$ as given by the first 3 terms of Eq. (12) by plotting the fractional difference between $\mathcal{C}(z_d)$ as given by Eq. (12) and $\mathcal{C}(z_d)$ as given by Eq. (11) for the indicated cosmologies. For lenses of redshift up to 0.5 the series approximation is accurate to 1%. In Fig. 4 we plot, for flat Λ CDM models, the fractional change in $\mathcal{C}(z_d)$ for various $(\Omega_m, \Omega_\Lambda)$ values compared to $\mathcal{C}(z_d)$ for the $(0.3, 0.7)$ universe. From the plots in the left panel we see that $\mathcal{C}(z_d)$ is more sensitive to Ω_m at smaller redshifts, and from the red curves on the right we see the uncertainty in measurement of the curvature term scales roughly linearly with that in Ω_m . Combining these observations with Fig. 3 we see that the series approximation should be accurate enough to determine Ω_m up

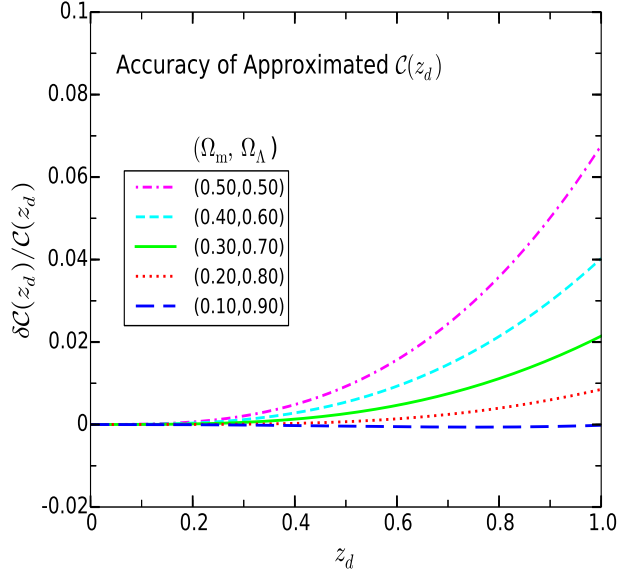


FIG. 3. The fractional difference of the series approximation for $\mathcal{C}(z_d)$ as given by Eq. (12) and the exact value as given by Eq. (11) is plotted for five flat cosmologies (from top to bottom): $(\Omega_m, \Omega_\Lambda) = (0.50, 0.50)$, dot-dashed magenta; $(0.40, 0.60)$ dashed cyan; $(0.30, 0.70)$ solid green; $(0.20, 0.80)$ dotted orange; $(0.10, 0.90)$ dashed blue.

to about 2% at redshifts up to $z_d \approx 0.7$ if the Universe is in the neighborhood of $(0.3, 0.7)$.

The blue curves plotted in the right panel of Fig. 4 and the curves plotted in Fig. 5 compare curvature functions of Eq. (11) for the concordance Λ CDM universe with universes whose Λ like field has a dynamical equation of state $p_\Lambda/\rho_\Lambda c^2 = [w_0 + w_a z/(1+z)]$. We have varied (w_0, w_a) about $(-1, 0)$ keeping $(\Omega_m, \Omega_\Lambda) = (0.3, 0.7)$ without placing any physical constraint on their values. For the range of variation of the two parameters shown, the maximum sensitivity is only reached beyond $z_d = 1$.

Cosmic voids identified through galaxy surveys generally have low redshifts $z \lesssim 0.5$ [43, 44], and as can be seen in Eq. (12) and the right panel of Fig. 2, at small redshifts the curvature term is dominated by the mass density parameter Ω_m . Consequently, this test should place its strongest constraint on Ω_m .

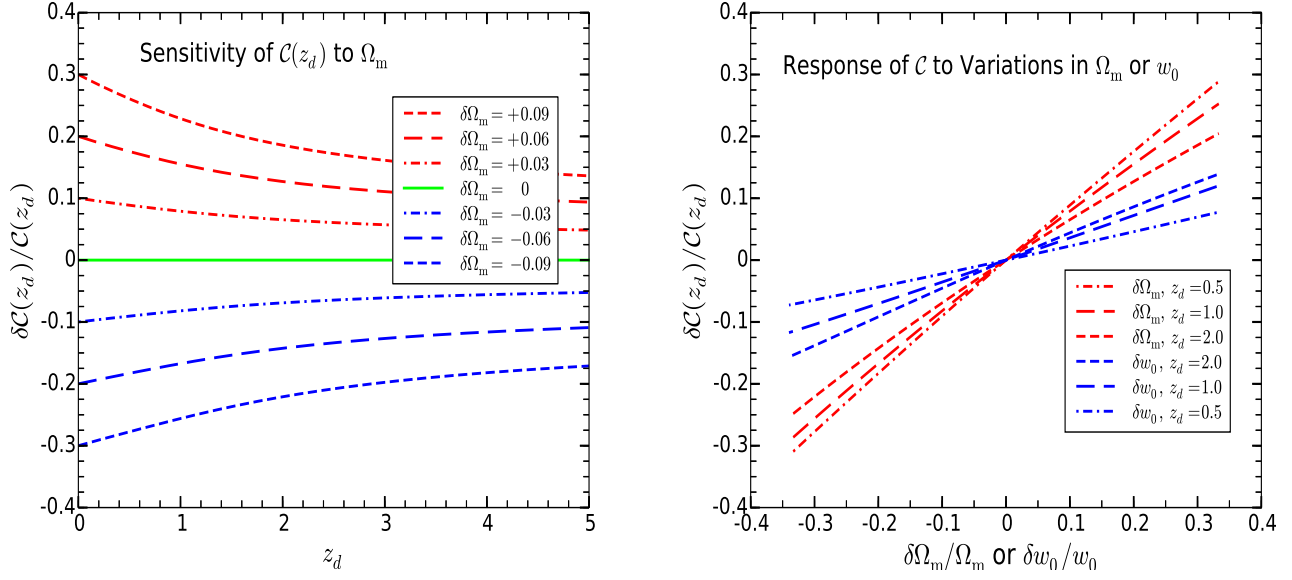


FIG. 4. (Left) Sensitivity of $\mathcal{C}(z_d)$ to the matter density parameters Ω_m . The fractional change in the curvature $\mathcal{C}(z_d)$ given by Eq. (11) is plotted as a function of the redshift z_d for several flat Λ CDM cosmologies close to $\Omega_m = 0.3$, i.e., $\delta\mathcal{C}/\mathcal{C} \equiv [\mathcal{C}(0.3 + \delta\Omega_m) - \mathcal{C}(0.3)]/\mathcal{C}(0.3)$ is plotted for $\delta\Omega_m = 0, \pm 0.03, \pm 0.06$, and ± 0.09 . (Right) The linear response of the curvature term (relative to the fiducial Λ CDM cosmology) as a function of variations of Ω_m for lens redshift $z_d = 0.5, 1.0$, and 2.0 (respectively dot-dashed, long dashed, and dashed curves) is plotted as the three red curves (larger slopes). The three blue curves (smaller slopes) are similarly produced by variations of w_0 about $w_0 = -1$. For a lens at redshift $z_d \approx 1$, a measurement of \mathcal{C} within 10% constrains Ω_m and w_0 up to about 12% and 25%, respectively.

III. EXAMPLES

The structure term $\mathcal{S}(\theta_I, z_d)$ has to be accurately modeled before we can use either of the two tests presented in the previous section to constrain the cosmological parameters. Modeling strong gravitational lenses (galaxies or clusters of galaxies) traditionally requires only the density profiles $\rho(\mathbf{r})$ of the lenses, whereas modeling ISW effects requires the additional knowledge of the first time derivative of $\rho(\mathbf{r})$ at lensing (equivalent to the first derivative with respect to z_d). Even if we assume that galaxy clusters are virialized, their density contrasts with respect to the FLRW background evolve with redshift, and so do their projected fractional mass profiles $f(x, z_d)$. To numerically evaluate Fermat potentials for compen-

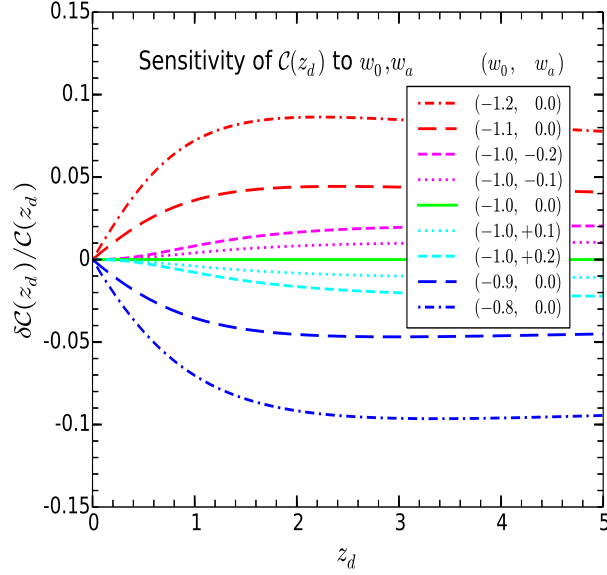


FIG. 5. Sensitivity of $\mathcal{C}(z_d)$ to the dark energy parameters w_0 and w_a . For all plotted cosmologies $(\Omega_m, \Omega_\Lambda) = (0.3, 0.7)$ but w_0 and w_a are allowed to respectively vary about -1 and 0, i.e., we test for $\delta w_0 = 0, \pm 0.1, \pm 0.2$, and $\delta w_a = 0, \pm 0.1, \pm 0.2$. The curvature term $\mathcal{C}(z_d)$ is more sensitive to variations in w_0 than w_a , see Eq. (12).

sated cluster lens models with realistic profiles, e.g., cluster lenses with profiles such as the embedded Navarro-Frenk-White (NFW) profile [45] is straight forward but analytical evaluation is challenging. Dark matter density profiles for cosmic voids are currently estimated by stacking and averaging galaxy counts over large numbers of voids. This assumes that luminous matter as tracers of dark matter is not significantly biased and even if correct, far less is known about void evolution than about cluster evolution. There are hints indicating that voids can be deep in the central regions, with $\delta \lesssim -0.8$ near the void center [42]. If this is indeed the case, then δ might be evolving very slowly (already approaching its lower bound of -1) and the z_d dependence in $f(x, z_d)$ might be negligible. If so the structure term would consequently be easier to model. Voids would simply be expanding with the background and the ISW effect would be determined by the time-delay contribution alone [22]. The ISW-z test might be more fruitfully applied to cosmic voids than galaxy clusters because it is very sensitive to cluster accretion (see below) and the CMB temperature seen through a cluster is contaminated by hot gas emissions from the cluster itself and from other

secondary anisotropies such as the Sunyaev-Zeldovich (SZ) effect [46, 47].

As a first attempt to illustrate the procedure of constructing the structure term $\mathcal{S}(z_d)$, we approximate cosmic density perturbations by a two-parameter family of either top-hat models for clusters or inverted top-hat models for voids, see Fig. 6. Both the cluster and void models are compensated with density profiles defined as

$$\frac{\rho - \bar{\rho}}{\bar{\rho}} = \begin{cases} \delta & , 0 \leq x < \mathbf{a}, \\ -\delta/(\mathbf{a}^{-3} - 1) & , \mathbf{a} \leq x < 1, \end{cases} \quad (13)$$

where $\bar{\rho}$ is the cosmic mean at the lens redshift, the parameter \mathbf{a} delineates the over and under-dense regions, and $-1 \leq \delta \leq (\mathbf{a}^{-3} - 1)$ is the density contrast of the inner region. When δ is negative this is a void model and when positive a model for an overdensity. The density contrast of the outer region ($\mathbf{a} < x \leq 1$) is entirely determined by the necessity of compensating for the excess/depleted central density. For this simple top-hat lens model we find

$$\int_0^1 \frac{f(x', z_d) - f_{\text{RW}}(x')}{x'} dx' = -\delta \frac{\log \mathbf{a}}{(\mathbf{a}^{-3} - 1)}, \quad (14)$$

and the structure term from Eq. (6) is

$$\mathcal{S}(z_d) = -\frac{\delta \log \mathbf{a}}{(\mathbf{a}^{-3} - 1)} - (1 + z_d) \frac{\log \mathbf{a}}{(\mathbf{a}^{-3} - 1)} \frac{d\delta}{dz_d} - (1 + z_d) \delta \frac{d}{dz_d} \left[\frac{\log \mathbf{a}}{(\mathbf{a}^{-3} - 1)} \right]. \quad (15)$$

If the lens does not evolve in co-moving space, i.e., if δ and \mathbf{a} are both constants, the density perturbation is not evolving in size or shape relative to the background cosmology and $\mathcal{S}(z_d)$ is just a constant given by Eq. (14). We refer to this non-evolving, i.e., co-expanding, value as S_0 , see the horizontal dashed brown curve in Fig. 7. If the density perturbation evolves relative to the FLRW background then δ and/or \mathbf{a} are functions of the deflectors redshift z_d , the quantity given by Eq. (14) evolves with time, and the additional derivative terms in Eq. (15) are present. The structure term $\mathcal{S}(z_d)$ will depend on the background cosmological parameters if either of the two parameters δ or \mathbf{a} does. If δ evolves but \mathbf{a} does not the second term is present and the perturbation's amplitude evolves relative to the background cosmology but the perturbation doesn't change its shape. Linear perturbations are of this type (see the four cosmological parameter dependent curves in Fig. 7). If \mathbf{a} evolves the last term is present and the shape of the perturbation evolves. Relaxed clusters (see Fig. 8) and voids produced by explosive motion are of this type [48–50]. We next discuss linear perturbations and relaxed clusters in more detail.

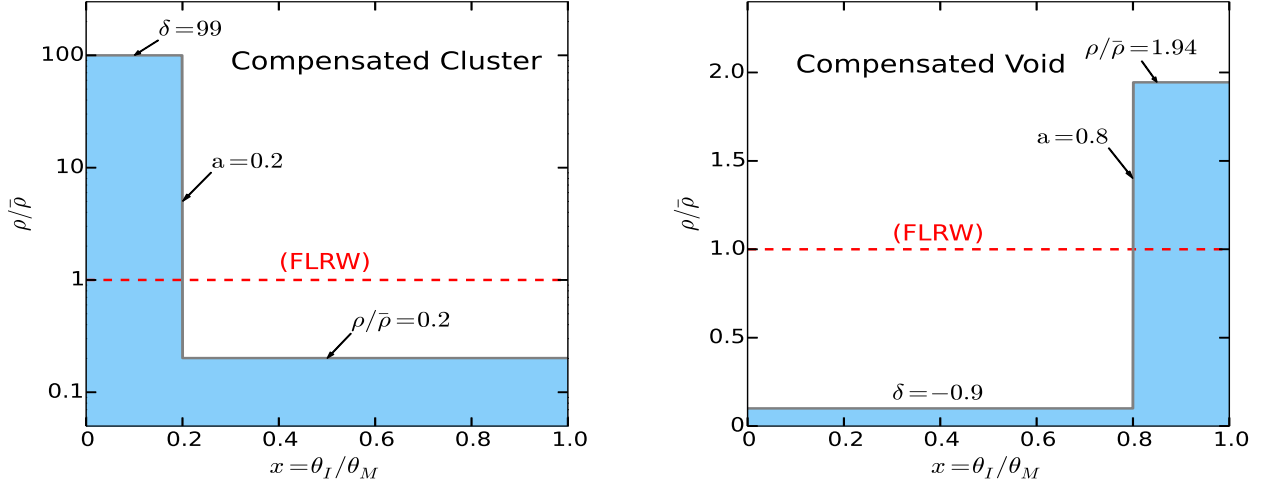


FIG. 6. Compensated top-hat models for a cluster on the left $a = 0.2, \delta = 99$ and a void on the right $a = 0.8, \delta = -0.9$. The well surrounding the cluster (and the wall surrounding the void) begins at physical radius $r = a r_d$.

A. Linearly Evolving Cosmic Voids and Large Scale Overdensities

As a first example of the ISW-z test using Eq. (7) we assume linear growth for the clusters or voids of the form given in Eq. (13). The fractional comoving radius of the top-hat remains constant ($a = a_0$) while δ evolves as

$$\delta = D_+(z_d) \delta_0, \quad (16)$$

where the linear perturbation growth factor [51]

$$D_+(z) = E(z) \int_z^\infty \frac{(1+z')}{[E(z')]^3} dz' \bigg/ \int_0^\infty \frac{(1+z')}{[E(z')]^3} dz', \quad (17)$$

depends on the cosmological parameters through $E(z)$, see Eq. (9). Consequently, linear evolution produces an evolving structure dependent term $\mathcal{S}(z_d)$ that depends on cosmological parameters such as Ω_m and Ω_Λ ,

$$\mathcal{S}(z_d) = -\delta_0 \frac{\log a_0}{(a_0^{-3} - 1)} \left[D_+(z_d) + (1+z_d) \frac{dD_+(z_d)}{dz_d} \right]. \quad (18)$$

In Fig. 7 we have plotted $\mathcal{S}(z_d) \div [-\delta_0 \log a_0 / (a_0^{-3} - 1)]$ for the top-hat cluster/void models of Eq. (13) to illustrate evolution of the structure parts of Eqs. (5) and (7). To obtain the

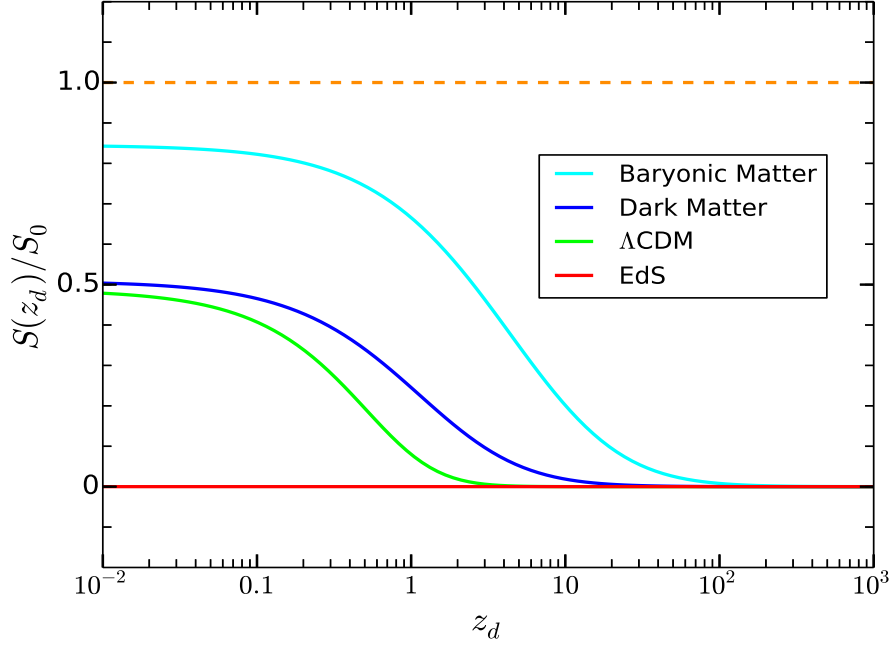


FIG. 7. Plots of the redshift evolution of the structure function $\mathcal{S}(z_d)/\mathcal{S}_0$ where $\mathcal{S}_0 \equiv -\delta_0 \log \mathbf{a}_0/(\mathbf{a}_0^{-3} - 1)$ for cluster ($\mathcal{S}_0 > 0$) and void ($\mathcal{S}_0 < 0$) models, see Eq. (13). The dashed brown curve is for cluster or void lenses co-expanding with the background cosmology. The solid curves are computed assuming linear evolution in four background cosmologies (bottom to top): the Einstein de Sitter universe, $(\Omega_m, \Omega_\Lambda) = (1, 0)$, red; a Λ CDM universe, $(\Omega_m, \Omega_\Lambda) = (0.3, 0.7)$, green; a dark matter only universe, $(\Omega_m, \Omega_\Lambda) = (0.3, 0)$, blue; and a baryonic-matter only universe, $(\Omega_m, \Omega_\Lambda) = (0.05, 0)$, cyan.

z_d dependence of the structure part for a particular lens simply multiply each curve by the appropriate value of $\mathcal{S}_0 \equiv [-\delta_0 \log \mathbf{a}_0/(\mathbf{a}_0^{-3} - 1)]$. To understand why the various evolutionary schemes produce different central temperatures at $z_d = 0$ for exactly the same perturbation density at $z_d = 0$, one has only to identify the two sources of the z_d dependence in Eq. (6). When the derivative acts on the $(1 + z_d)$ term the contribution to Eq. (4) is $H_d T_p/(1 + z_d)$ which is directly proportional to the potential part of the lensing time delay T_p . At the delayed exit, time the background CMB photons have further cooled and reddened whereas the lensed CMB photons, stuck in the lens, were not so reddened, and hence appear relatively bluer. This time-delay contribution to the temperature shift of the CMB is common to all evolutionary schemes and constitutes the entire temperature shift if the lens mass structure

is evolving exactly like the background cosmology, i.e., co-expanding. If the lens density evolves differently than the background, transiting CMB photons can lose or gain energy by virtue of the changing depth of the transited gravitational potential within the lens. If the lens is more condensed in the past, $\partial f(x, z_d)/\partial z_d > 0$ in Eq. (6), the fractional projected lens mass $f(x, z_d)$ decreased with cosmic time and transiting photons lose less energy when climbing out of the lens' potential well than they gain when falling in. They would thus appear even bluer because of the evolution. However, if $\partial f(x, z_d)/\partial z_d < 0$, the lens structure is becoming more condensed with time (as shown in Fig. 7 for linear perturbations) and the CMB photons are redshifted because of evolution. The larger the evolution rate the more reduction takes place in the time-delay blue shift. In the EdS universe $D_+(z_d) \propto R(t_d)$ assuming linear evolution (see Eq. (18)), and the evolution reddening completely cancels the time-delay blue shift (see the solid red curve in Fig. 7). See Chen et al. [22] for more discussion about the time-delay and evolutionary contributions to the ISW effect.

B. Virialized Clusters

We evaluate the structure function $S(z_d)$ for four cluster models, one completely static, one co-expanding, and two virialized but accreting (see Table 1). A virialized cluster model of the top-hat form given in Eq. (13) that has stopped evolving, i.e., one that is completely static, would have a constant physical radius r_a and a constant central density ρ_c , or equivalently a z -dependent comoving radius

$$a = \frac{r_a}{r_d(z)} = a_0(1+z), \quad (19)$$

and a z -dependent central density enhancement

$$1 + \delta(z) \equiv \frac{\rho_c}{\bar{\rho}(z)} = (1 + \delta_0)(1+z)^{-3}. \quad (20)$$

The mass contained in the cluster is

$$M_c(z) = \frac{4}{3} \pi r_a^3 \rho_c = a^3 [1 + \delta(z)] M_d, \quad (21)$$

where $M_d = 4/3 \pi r_d^3 \bar{\rho}(z)$ is the (constant) mass contained in the co-moving Swiss cheese sphere from which the cluster condensed. The mass remaining in the depleted region around the cluster is simply $(M_d - M_c)$ and is the source of the accreting mass. If the cluster wasn't

virialized but simply co-expanding with the background cosmology, \mathbf{a} and the central density enhancement $1 + \delta$ would both remain constant. For either of these two scenarios: model I. A static with constant physical radius $r_{\mathbf{a}}$ and constant central density ρ_c or model II. A co-expanding cluster with constant fractional comoving radius \mathbf{a} and constant central density contrast δ , the mass of the central cluster remains constant. Even though there are no observational measurements of mass accretion rates for clusters, they are all widely believed to be accreting mass. To use the simple two-component mass profile models of the form given in Eq. (13) to estimate the effect of accretion on the structure function $\mathcal{S}(z_d)$ we allow mass from the depleted background material surrounding the cluster ($r_{\mathbf{a}} \leq r \leq r_d$), whose mass density is $[1 - \delta/(\mathbf{a}^{-3} - 1)] \times \bar{\rho}$, and who's partially depleted contents previously collapsed to form the cluster, to be continually falling onto that cluster after virialization at some specified rate

$$\frac{dM_c}{dt} = -(1+z)H_d \frac{dM_c}{dz}. \quad (22)$$

If mass accretes, \mathbf{a} and/or $\delta(z)$ differ from the values given by Eqs. (19) and/or (20). To make use of current accretion rate estimates we choose two accreting scenarios: the first, model III. Keep the central density contrast fixed with $\rho_c(z) = (1+\delta)\bar{\rho}(z) = 200\bar{\rho}(z)$ and let the comoving radius $\mathbf{a}(z)$ increase with cosmic time (decrease with redshift), see Eq. (21). In the second accreting scenario, model IV. Assume the physical radius $r_a = \mathbf{a}(z)r_d(z)$ remains constant while the central density enhancement $1+\delta(z)$ increases with time to accommodate the accreting mass. A comparison of these four simple cluster models is shown in Table I.

Even though there is no observational data giving dM_c/dz for accreting clusters, there are several fitting formulae arrived at by using the extended Press-Schechter formalism and N-body simulations to estimate that rate. Two such simple fitting formulae are 2-parameter expressions due to McBride et al [53]

$$M_c(z)/M_c(0) = (1+z)^\beta e^{-\gamma z}, \quad (23)$$

and van den Bosch [54]

$$M_c(z)/M_c(0) = \exp \left\{ \ln(1/2) \left[\frac{\ln(1+z)}{\ln(1+z_f)} \right]^\nu \right\}. \quad (24)$$

These models are designed to represent stochastic averages of field galaxies and groups merging with the cluster and increasing its mass at the specified rate. Other fitting formulas

TABLE I. Cluster models

Model	M_c constant	r_a constant	a constant	δ constant	descriptions
I	yes	yes	no	no	non-accreting static
II	yes	no	yes	yes	non-accreting co-expanding
III	no	no	no	yes	accreting with fixed δ
IV	no	yes	no	no	accreting with fixed r_a

can be found in [55, 56]. Estimates of the parameters (β, γ) and (z_f, ν) can be found in [57] for the conventional Λ CDM background.

In Fig. 8 we estimate the effect of mass accretion, Eq.(22), on the structure function $\mathcal{S}(z_d)$ of clusters by assuming mass accretion histories of the form Eqs.(23) and (24). Because of the limited availability of fitting data we choose for all four cases shown, a cluster mass of $M_c(0) = 10^{15} M_\odot$ at $z = 0$ and a central density enhancement $1 + \delta_0 = 200$ at $z = 0$ in a concordance background. We take $(\beta, \gamma) = (-0.690, 1.280)$ and $(z_f, \nu) = (0.381, 1.252)$ in Eqs. (23) and (24) respectively from fits found in [57].

The top four curves give $\mathcal{S}(z_d)$ of Eq. (6) for non-accreting (constant cluster mass M_c) models I and II, the static and co-expanding models (black and green curves respectively). The thick lines are cluster models whose cluster mass $M_c(z)$ at $z = 0$ is 1/10 of the Swiss cheese void's constant mass M_d (the mass of the homogeneous sphere from which the cluster condensed). The thin lines are for smaller void masses, $M_d = 2M_c(0)$ with correspondingly smaller radii $\propto (2/10)^{1/3}$.

The blue and red curves in Fig. 8 are computed assuming the McBride and van den Bosch accretion histories of Eqs.(23) and (24) respectively. The solid and dashed curves are for constant central density contrast δ (model III) and constant physical radius r_a (model IV) respectively, see Table 1. For $z \leq 0.1$ estimated values of $\mathcal{S}(z_d)$ cannot be accurate because the fitted values of $dM(z)/dz$ differ significantly between Eqs. (23) and (24). In general the mass accreted while the CMB photons transit the cluster deepens the potential well from which the photons must climb to reenter the background cosmology. They are thus reddened by accretion. As can be seen in Fig.8 the effect of accretion seems to dominate the ISW effect for cluster centers.

The large negative values of $\mathcal{S}(z_d)$ seen in Fig.8 for the two accreting cluster models

III and IV are highly uncertain but are clearly worrisome since they would make the CMB temperature in the center of the cluster much cooler than expected, and would even produce a central cold spot. This is in contrast to conventional wisdom that galaxy clusters produce CMB hot spots at $z \lesssim 1$ because the accelerated expansion of the Universe reduces the depth of the potential well from which the transiting photons must climb. We find that when accretion is happening its effects can overwhelm the effects of acceleration, i.e., the potential well might be deepening inspite of the acceleration. Of course the accuracy of the predictions made by these models can be questioned because they assume continuous accretion whereas the consensus is that mass accretes via discrete mergers of halos associated with galaxies groups ($\leq 10^{13}M_\odot$) and/or galaxies ($\leq 10^{12}M_\odot$). To estimate the reasonableness of the continuous accretion model we compare the photon's lensing time with the time between mergers. The time it takes a photon to cross the Swiss cheese void is $\sim 2.5 \times 10^{-1}$ Gyr for a $10^{15}M_\odot$ cluster lens with $M_d/M_c(0) = 10$ and $\sim 1.5 \times 10^{-1}$ Gyr when $M_d/M_c(0) = 2$. Time between mergers is $\sim 7 \times 10^{-3}$ Gyr for galaxies and $\sim 7 \times 10^{-2}$ Gyr for groups. If only galaxies were accreting then ~ 35 (21 for $M_d/M_c(0) = 2$) would merge while the photon transited the lens whereas if groups were responsible for the mass accretion only ~ 3.5 (2.1 for $M_d/M_c(0) = 2$) would have merged. The time taken for photons to cross the central cluster itself is only $\sim 2.0 \times 10^{-2}$ Gyr; however, it is the change of the potential across the entire compensated lens that determines the ISW temperature shift, i.e., transiting CMB photons have to make their way across the large continually depleting low density compensating region before reentering the background cosmology. We consider two extreme physical pictures in the following. A more realistic picture would be a combination of the two. If $10^{15}M_\odot$ clusters assemble their masses by accreting only $10^{12}M_\odot$ galaxies there would be ~ 1000 galaxies in the cluster and ~ 9000 galaxies surrounding the cluster in the low density compensating region (for the $M_d = 10M_c(0)$ Swiss cheese lens). During the time it took the CMB photons to cross the entire lens ~ 35 galaxies would have accreted from the compensating region to the central cluster. If clusters assembled their masses by accreting $10^{13}M_\odot$ groups, all numbers would be decreased by a factor of 10. If the low density compensating region surrounding the cluster was smaller, i.e., if $M_d = 2M_c(0)$ then there would be only 1000 galaxies in the compensating region and during the CMB crossing only ~ 21 galaxies would have accreted. The current state of accretion theory, as judged by Fig. 8, clearly suggests that Eq. (5) is more likely to constrain cluster structure and evolution

than cosmology at this time. If accurate density profiles can be constructed, combined with additional measurements of central cluster temperatures deficits one should be able to put limits on cluster mass accretion rates.

IV. CONCLUSIONS

The ISW effect has been recently detected via the aperture photometry method (stacking/averaging patches of the CMB maps around known cosmic voids or galaxy clusters) by several groups [3, 5, 9–11] and future observations promise more and better data. We present a new method of using this data to potentially constrain the cosmological parameters by applying the ISW effect to individual inhomogeneities such as galaxy clusters and cosmic voids. We were able to develop this ISW-redshift test only after discovering a simple relation between the Fermat potential of an embedded lens and the frequency shift of photon crossing that lens. However, to use this test to extract the Hubble parameter and/or the curvature parameters the evolution of the lens has to be well understood. We have illustrated use of the ISW-z test by constructing models for clusters and voids with very simple density profiles and simple evolutions (i.e., top-hats for linearly evolving clusters/voids and completely virialized clusters with and without accretion). However, for both galaxy clusters and cosmic voids, neither their density profiles nor their time evolution is currently well enough constrained by observations to be used in this test. Consequently, the proposed ISW-z test might be more appropriately used to measure structure functions $\mathcal{S}(z_d)$, and constrain dark matter profiles, evolution, and accretion by assuming a specific cosmology and using the CMB observations. There are several theoretical/numerical papers modeling the formation and evolution of cosmic voids [48–50, 58] which can be used to estimate the structure term $\mathcal{S}(\theta_I, z_d)$ of Eq. (6) and the ISW-z test can possibly confirm or reject such models as more data becomes available. The density profile of galaxy clusters is thought to be much better constrained than profiles of cosmic voids, and for their low redshift evolution it is reasonable to assume that they are virialized. However, as seen in Fig. 8 the structure term $\mathcal{S}(\theta_I, z_d)$ is sensitive to the accretion rate which is poorly understood. What is clear from Fig. 8 is that accretion can make the centers of clusters appear unexpectedly cool just as is currently being seen [59]. Obviously better models for cosmic voids and galaxy clusters are needed

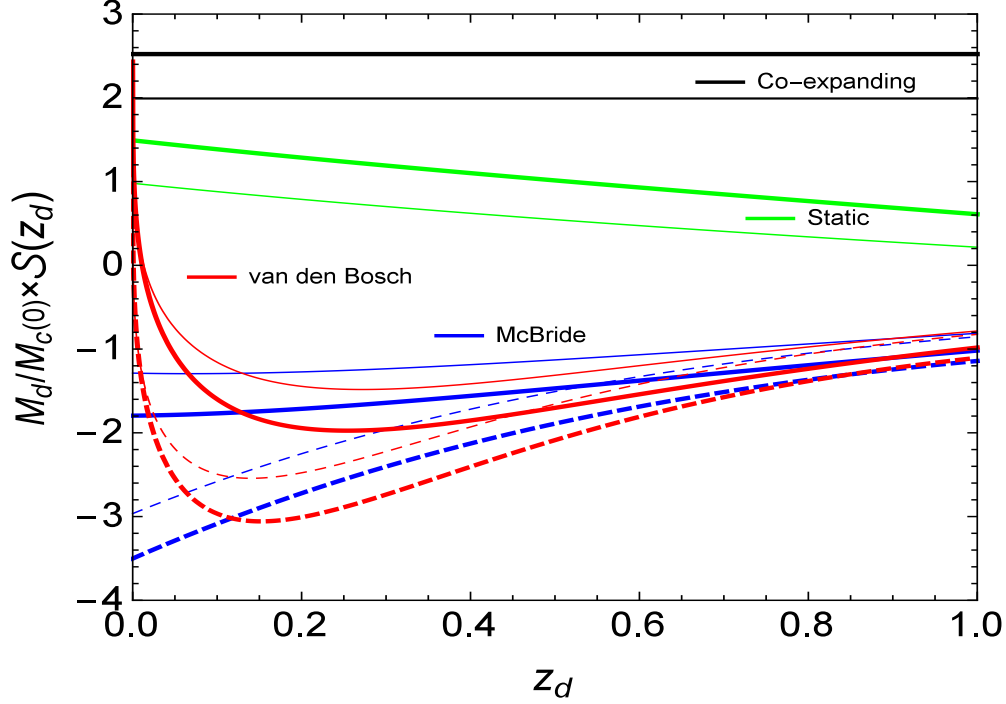


FIG. 8. Structure function $S(z_d)$ for four cluster models from Table 1. The effect of mass accretion on $M_d/M_c(0) \times S(z_d)$ in the flat Λ CDM background cosmology is plotted for clusters whose mass at $z = 0$ is $M_c(0) = 10^{15} M_\odot$. The $M_d/M_c(0)$ factor is included for the purpose of comparing $\Delta\mathcal{T}$'s of Eq. (5) because $r_s \propto M_d$. Thick lines are for clusters condensed from homogeneous spherical regions containing a total mass $M_d = 10 M_c(0)$, and thin lines for $M_d = 2 M_c(0)$. Consequently clusters in larger lenses (thick curves) have smaller fractional radii a resulting in different $S(z_d)$ values, see Eq. (15). The two top horizontal black curves are for co-expanding non-accreting clusters and the next two straight green lines are for static non-accreting clusters. The curved lines are accreting models. Blue models accrete according to [53] (McBride) and red models according to [54] (van den Bosch). The solid line models assume the cluster's central density enhancement remains at $(1 + \delta) = 200$ during accretion and the physical radius r_a increases. The dashed line models assume the physical radii r_a remain constant and the central density enhancements $1 + \delta(z)$ increase with time. Even though accretion histories described by Eqs. (23) and (24) are very similar, the associated accretion rates are very different near $z \sim 0$ and estimated values for $S(z_d)$ based on these rates, clearly, cannot be trusted for $z_d < 0.1$.

before the ISW-z test will constrain the cosmological parameters.

-
- [1] R. K. Sachs and A. M. Wolfe, *Astrophys. J.* **147**, 73 (1967).
 - [2] M. J. Rees and D. W. Sciama, *Nature (London)* **217** 511 (1968).
 - [3] B. R. Granett, M. C. Neyrinck, & I. Szapudi, *Astrophys. J. Lett.* **683**, 99 (2008a).
 - [4] B. R. Granett, M. C. Neyrinck, & I. Szapudi, arXiv.0805.2974 (2008b).
 - [5] Planck Collaboration, P. A. R., Ade, et al., *Astron. Astrophys.* **571**, 19, arXiv1303.5079 (2014).
 - [6] K. T. Inoue & J. Silk, *Astrophys. J.* **648**, 23 (2006).
 - [7] L. Rudnick, S. Brown, & L. R. Williams, *Astrophys. J.* **671**, 40 (2007).
 - [8] S. Nadathur, S. Hotchkiss, & S. Sakar, *JCAP* **06**, 042 (2012).
 - [9] C. Hernández-Monteagudo, *Astron. Astrophys.* **520**, 101 (2010).
 - [10] S. Ilić, M. Langer, & M. Douspis, *Astron. Astrophys.* **556**, 51 (2013).
 - [11] Y-C. Cai, M. C. Neyrinck, I. Szapudi, S. Cole & C. S. Frenk, *Astrophys. J.* **786**, 110 (2014).
 - [12] G. Lavaux & B. D. Wandelt, *Astrophys. J.* **754**, 109 (2012).
 - [13] J-B. Melin & J. G. Bartlett, arXiv1408.5633 (2014).
 - [14] U. Chantavat, U. Sawangwit, P. M. Sutter, & B. D. Wandelt, arXiv.1409.3364 (2014).
 - [15] N. Hamaus, P. M. Sutter, G. Lavaux, & B. D. Wandelt, *JCAP* **12**, 013 (2014).
 - [16] J. H. Cooke & R. Kantowski, *Astrophys. J. Lett.* **195**, 11 (1975).
 - [17] R. Kantowski, B. Chen, and X. Dai, *Astrophys. J.* **718**, 913 (2010).
 - [18] B. Chen, R. Kantowski, and X. Dai, *Phys. Rev. D* **82**, 043005 (2010).
 - [19] B. Chen, R. Kantowski, and X. Dai, *Phys. Rev. D* **84**, 083004 (2011).
 - [20] R. Kantowski, B. Chen, and X. Dai, *Phys. Rev. D* **86**, 043009 (2012).
 - [21] R. Kantowski, B. Chen, and X. Dai, *Phys. Rev. D* **88**, 083001 (2013).
 - [22] B. Chen, R. Kantowski, and X. Dai, *Astrophys. J.*, submitted, arXiv1310.6351 (2013).
 - [23] B. Chen, R. Kantowski, and X. Dai, *Astrophys. J.*, in press, arXiv1310.7574 (2013).
 - [24] A. Einstein and E. G. Strauss, *Rev. Mod. Phys.* **17**, 120 (1945).
 - [25] E. Schücking, *Z. Phys.* **137**, 595 (1954).
 - [26] R. Kantowski, *Astrophys. J.* **155**, 89 (1969).
 - [27] G. Lemaitre, *Ann. Soc. Bruxelles* **A53**, 51 (1933).

- [28] R. C. Tolman, Proc. Natl. Acad. Sci. **20**, 169 (1934).
- [29] H. Bondi, Mon. Not. R. Astron. Soc. **107**, 410 (1947).
- [30] L. Nottale, Mon. Not. R. Astron. Soc. **206**, 713 (1984).
- [31] E. Martínez-González, J. L. Sanz, & J. Silk, Astrophys. J. Lett. **355**, 5 (1990).
- [32] M. Panek, Astrophys. J. **388**, 225 (1992).
- [33] U. Seljak, Astrophys. J. **460**, 549 (1996).
- [34] N. Sakai, & K. T. Inoue, Phys. Rev. D **78**, 063510 (2008).
- [35] W. Valkenburg, JCAP **06**, 010 (2009).
- [36] P. Schneider, J Ehlers, and E. E. Falco, *Gravitational Lenses* (Springer-Verlag, Berlin, 1992).
- [37] A. Cooray, Phys. Rev. D **65**, 083518 (2002).
- [38] B. M. Schäfer & M. Bartelmann, Mon. Not. R. Astron. Soc. **431**, 425 (2006).
- [39] P. M. Merkel & B. M. Schäfer, Mon. Not. R. Astron. Soc. **431**, 2433 (2013).
- [40] M. Birkinshaw & S. F. Gull, Nature (London) **302**, 315 (1983).
- [41] L. I. Gurvits & I. G. Mitrofanov, Nature (London) **324**, 349 (1986).
- [42] P. M. Sutter, G. Lavaux, B. D. Wandelt, & D. H. Weinberg, Astrophys. J. **761**, 44 (2012).
- [43] K. N. Abazajian, et al. Astrophys. J. Suppl. Ser. **182**, 543 (2009).
- [44] P. M. Sutter, G. Lavaux, B. D. Wandelt, D. H. Weinberg, & M. S. Warren, Mon. Not. R. Astron. Soc. **438**, 3177 (2014).
- [45] J. F. Navarro, C. S. Frenk, & S. D. White, Astrophys. J. **462**, 563 (1996).
- [46] R. A. Sunyaev, & Y. B. Zeldovich, Mon. Not. R. Astron. Soc. **190**, 413 (1980).
- [47] M. Birkinshaw, PhR **310**, 97 (1999).
- [48] J. P. Ostriker, & L. L. Cowie, Astrophys. J. Lett. **243**, 127 (1981).
- [49] E. Bertschinger, Astrophys. J. Suppl. Ser. **58**, 1 (1985a).
- [50] E. Bertschinger, Astrophys. J. Suppl. Ser. **58**, 39 (1985b).
- [51] D. J. Heath, Mon. Not. R. Astron. Soc. **179**, 351 (1977).
- [52] G. L. Bryan & M. L. Norman, Astrophys. J. **495**, 80 (1998).
- [53] J. McBride, O. Fakhouri, & C.-P. Ma, Mon. Not. R. Astron. Soc. **398**, 1858 (2009).
- [54] F. C. van den Bosch, Mon. Not. R. Astron. Soc. **331**, 98 (2002).
- [55] J. R. Bond, S. Cole, G. Efstathiou, & N. Kaiser, Astrophys. J. **379**, 440 (1991).
- [56] C. Lacey & S. Cole, Mon. Not. R. Astron. Soc. **262**, 627 (1993).
- [57] C. De Boni, A. L. Serra, A. Diaferio, C. Giocoli, & M. Baldi, arXiv1501.01977 (2015).

- [58] R. K. Sheth, & R. van de Weygaert, *Mon. Not. R. Astron. Soc.* **350**, 517 (2004).
- [59] Planck Collaboration, P. A. R., Ade, et al., arXiv1502.01595 (2015).